

Geophysical Research Letters

RESEARCH LETTER

10.1029/2020GL089689

Key Points:

- The 2019 cold surge in Midwest USA is not isolated; it is a cooling phase sandwiched within two warming phases as a stationary wave train
- Though initially triggered by the southward Arctic air, the cold surge grows explosively due to a very strong baroclinic instability
- The synchronization between wind perturbation and temperature perturbation provides a precursor for the cold surge at a lead time of 5 days

Supporting Information:

- Supporting Information S1
- Movie S1

Correspondence to:

X. S. Liang,
sanliang@courant.nyu.edu

Citation:

Xu, F., & Liang, X. S. (2020). The synchronization between the zonal jet stream and temperature anomalies leads to an extremely freezing North America in January 2019. *Geophysical Research Letters*, 47, e2020GL089689. <https://doi.org/10.1029/2020GL089689>

Received 9 JUL 2020

Accepted 8 SEP 2020

Accepted article online 21 SEP 2020

The Synchronization between the Zonal Jet Stream and Temperature Anomalies Leads to an Extremely Freezing North America in January 2019

Fen Xu^{1,2}  and X. San Liang^{1,2,3} 

¹School of Atmospheric Sciences, Nanjing University of Information Science and Technology, Nanjing, China, ²Center for Ocean-Atmosphere Dynamical Studies, Nanjing Institute of Meteorology, Nanjing, China, ³School of Marine Sciences, Nanjing University of Information Science and Technology, Nanjing, China

Abstract In late January 2019, a severe cold air outbreak brought the lowest temperatures in over 20 years to Midwestern United States and Eastern Canada. With a newly developed functional analysis tool, namely, multiscale window transform, and the multiscale window transform-based theory of canonical transfer, it is found, based on the data from National Center for Environmental Prediction, that the cold surge, though initialized by the southward migration of the Arctic air mass, is mainly caused by a synchronization between perturbation temperature and perturbation winds, which leads to a very strong baroclinic instability and hence an explosive growth of available potential energy on the cold surge scale window. The cold event is actually a part of a localized stationary wave train, sandwiched between two warming centers, over western North America and over Atlantic. The synchronization can serve as a precursor for this extremely severe cold surge.

Plain Language Summary The January 2019 cold air outbreak over North America resulted in an extremely freezing weather in the Midwest of the United States, incurring a heavy economic and life loss. In this study, we find that this cold surge is actually a phase sandwiched within two warming phases, and these phases make a whole for a quasi-stationary wave train. While it is believed that the southward migration of the Arctic air mass caused this event, we find that the Arctic air mass migration just initialized the cooling; it did not account for the extremely freezing weather and its persistence. The main cause is a very strong baroclinic instability of the jet stream, which leads to the formation of the wave train and the plummeting of the temperature. We also find that the synchronization between the wind perturbation and temperature perturbation actually heralds the arrival of the cold surge. It can serve as a precursor for this disastrous weather at a lead time of more than 5 days.

1. Introduction

In 2019, North America experienced its coolest January since 2011; a large-scale cold air outbreak (CAO) occurred in late January in the Midwest of the United States and, particularly, the Great Lakes region, with maximum temperatures during this time below -25.0°C (cf. <https://www.ncdc.noaa.gov/sotc/global/201901>). At least 22 people died because of the freezing weather, together with a lot of flight cancellations, public school closures, and so forth, incurring heavy casualties and economic losses (cf. <https://www.climate.gov/news-features/blogs/beyond-data/bitterly-cold-extremes-warming-planet-putting-midwests-late-january>).

CAO is a disastrous weather phenomenon in the midlatitudes of the Northern Hemisphere. It is generally associated with a surface anticyclone-cyclone couplet, between which cold air masses are transported from higher latitudes. Extreme CAO events will cause a persistent freezing weather that may severely affect the daily human being life and the economic activities therein (Lau & Lau, 1984), just as the January 2019 one did.

Climate models and observations both show that extreme cold events continue to persist on each continent despite the warming globe (Gao et al., 2015; Kodra et al., 2011), and this is particularly serious in North America (Walsh et al., 2001). For example, Van Oldenborgh et al. (2015) found the unusually long duration of cold conditions in the winter 2014. How the air masses are cumulatively cooled and,

particularly, maintained in a warming context is, therefore, both of societal relevance and of great scientific importance.

Much effort has been invested in explaining the generation of CAOs. From a thermodynamic point of view, Konrad and Colucci (1989) examined the role of cold advection and adiabatic heating in forming the two strong CAOs in eastern North America in January 1977, which is substantiated by Portis et al. (2005). Yu et al. (2015) showed that stronger warm air mass transport into the upper polar atmosphere is accompanied with stronger equatorward discharge of cold polar air in the lower troposphere, resulting in massive CAOs in midlatitudes and anomalous warmth in high latitudes. On the other hand, Harnik et al. (2016) examined a variety of large-scale extreme CAOs in North America and found that the tropospheric jet stream undulations may bring polar cold air over to the American continent, leading to the formation of the CAOs. Xie et al. (2019) emphasized the role of the planetary-scale and synoptic-scale waves, which collaborate to promote the occurrence of the cold events. But Konrad (1996, 1998) showed that the cold wave intensity is more related to planetary-scale circulation anomalies than synoptic-scale anomalies. Besides, CAO events are also found closely related to the North Atlantic Oscillation or Arctic Oscillation (Cattiaux et al., 2010; Cellitti et al., 2006; Walsh et al., 2001).

Recently, the role of stratosphere has caught much attention. Tomassini et al. (2012) showed that about 40% extreme cold spells may have their origins in the stratosphere—they are preceded by disturbances in the stratosphere. Cai et al. (2016) also confirmed that the probability of continental-scale CAOs is related to the amount of air mass transported into the polar stratospheric polar regions. Over recent decades, the stratospheric polar vortex has become weaker than before; Kretschmer et al. (2018) argued that this can be used to explain the cooling trend of the Eurasia in boreal winter.

The aforementioned mechanisms, though successful in explaining the generation of the CAOs in their specific context, may not be applicable for the January 2019 one, which last for nearly half a month. Its maintenance and, particularly, maintenance in the context of global warming may have some unusual dynamical processes lying behind. In this study, we are about to investigate these processes, using a newly developed functional analysis apparatus, namely, multiscale window transform (MWT), and the MWT-based theory of canonical transfer and multiscale energetics analysis. In the following, we first briefly introduce the data and the methodology, then perform multiscale analysis, and investigate the resulting multiscale phenomena and energetics. As we will see soon, the extreme CAO is indeed associated with an unusual synchronization of some MWT reconstructed fields, and the synchronization persists for more than half a month. This study is summarized in section 5.

2. Data and Method

2.1. Data

The National Centers for Environmental Prediction-National Center for Atmospheric Research reanalysis data, including temperature, geopotential, and wind (u , v , ω), are utilized for the purpose of this study. The data are in isobaric coordinates, with 17 pressure levels, from 1,000 to 10 hPa (but ω has only 12 levels, from 1,000 to 100 hPa). They have a horizontal resolution of $2^\circ \times 2^\circ$ and a resolution of 6 hr in time. The time series span from 22 March 2018 through 16 August 2019, totaling 512 days.

2.2. MWT

The research methodology for this study is the MWT by Liang and Anderson (2007) and the MWT-based theory of canonical transfer (Liang, 2016) and localized multiscale energy and vorticity analysis by Liang and Robinson (2005). Hereafter is just a brief introduction; more details are referred to Liang (2016).

Originally, Lorenz (1955) formulated the multiscale atmospheric energetics with Reynolds decomposition. However, Reynolds decomposition with respect to time (spatial dimension) does not have temporal (spatial) localization retained, while real atmospheric processes, the CAO process in particular, are in nature highly localized (nonstationary and/or inhomogeneous). To overcome the difficulty, the past three decades have seen wide applications of filters in place of the Reynolds decomposition in these analyses. But if energetics are to be studied, a very basic question arises: *What is the energy corresponding to a filtered field?* Essentially in all the filter-based formalisms so far, this problem has been overlooked; people simply take the square of a filtered field as the energy (up to some factor). Unfortunately, this is not the case even by concept.

To illustrate, suppose we have a field $u = u(t)$ (space dependence suppressed for simplicity), which is made of a slow process $\bar{u}(t)$ (with frequency ω_0) and a fast process $u'(t)$ (with frequency ω_1 , $\omega_1 > > \omega_0$):

$$u(t) = \bar{u}(t) + u'(t) = [a_0 \cos \omega_0 t + b_0 \sin \omega_0 t] + [a_1 \cos \omega_1 t + b_1 \sin \omega_1 t].$$

Take the fast process $u'(t)$ as an example. It can be easily obtained with a high-pass filter. By the common practice, its energy would be simply

$$[u'(t)]^2 = [a_1 \cos \omega_1 t + b_1 \sin \omega_1 t]^2.$$

This obviously differs from $a_1^2 + b_1^2$, the energy in Fourier space.

In fact, this is by no means a trivial problem. The common practice fails because general filters yield only reconstructions (i.e., filtered variables), lacking transform coefficients (like Fourier coefficients), and hence, there is no way to express the corresponding energies. In 2007, Liang and Anderson (2007) developed a mathematical apparatus which can function like a filter while producing transform coefficients as well. This is the MWT. MWT decomposes a function space into a direct sum of orthogonal subspaces, each with an exclusive range of scales, while retaining the locality of the resulting multiscale energies. Such a subspace is termed a *scale window* or simply a window. Given a scale window ϖ , for a time series $T(t)$, it can be reconstructed onto the window, written $T^{\sim\varpi}(t)$ (this is just like a filtered series). In the mean time, we have a transform coefficient, written $\hat{T}_n^{\sim\varpi}$ ($(\cdot)_n^{\sim\varpi}$ denotes MWT on window ϖ at time step n). The multiscale energy on window ϖ is then $[\hat{T}_n^{\sim\varpi}]^2$ (up to some multiplier). Note that it is by no means the square of the filtered field $[T^{\sim\varpi}(t)]^2$! This is where MWT differs from the traditional filters.

In MWT, a scale window is demarcated by two scale levels in the wavelet spectrum. Given a series $\{T(t)\}$ with a duration τ , a scale level j corresponds to a period $2^{-j}\tau$. Here we need three scale windows, which are bounded above by three scale levels, j_0 , j_1 , and j_2 , or by three time scale bounds, $2^{-j_0}\tau$, $2^{-j_1}\tau$, and $2^{-j_2}\tau$. For easy reference, they will be referred to as *background flow-scale window*, *CAO-scale window*, and *synoptic-scale window* and denoted by $\varpi = 0, 1, 2$, respectively.

2.3. Canonical Transfer and Multiscale Energetics Analysis

With MWT, the available potential energy (APE) and kinetic energy (KE) on window ϖ , respectively, denoted as A^{ϖ} and K^{ϖ} , at location n is

$$A^{\varpi} = \frac{1}{2} c (\hat{T}_n^{\sim\varpi})^2, \quad K^{\varpi} = \frac{1}{2} (\widehat{\mathbf{v}_h})_n^{\sim\varpi} \cdot (\widehat{\mathbf{v}_h})_n^{\sim\varpi},$$

where $\mathbf{v}_h = (u, v)$ is the horizontal velocity, T is the temperature anomaly (with the mean vertical profile $\bar{T}(z)$ removed), and $c = \frac{g}{\bar{T}(g/C_p - L)}$ is a constant of proportionality depending on the buoyancy frequency (L is lapse rate). Liang (2016) showed that, for window $\varpi (= 0, 1, 2)$, the energy equations are (for notational simplicity, the subscript n is suppressed henceforth)

$$\frac{\partial A^{\varpi}}{\partial t} = \underbrace{-\nabla \cdot \left[\frac{1}{2} c (\widehat{\mathbf{v}T})^{\sim\varpi} \hat{T}^{\sim\varpi} \right]}_{\Delta Q_A^{\varpi}} + \underbrace{\frac{1}{2} c \left[(\widehat{\mathbf{v}T})^{\sim\varpi} \cdot \nabla \hat{T}^{\sim\varpi} - \hat{T}^{\sim\varpi} \nabla \cdot (\widehat{\mathbf{v}T})^{\sim\varpi} \right]}_{\Gamma_A^{\varpi}} + \underbrace{\hat{\omega}^{\sim\varpi} \hat{\alpha}^{\sim\varpi}}_{-b^{\varpi}} \\ + \underbrace{\frac{1}{2} \hat{T}^{\sim\varpi} (\widehat{\mathbf{v}T})^{\sim\varpi} \frac{\partial c}{\partial p} + \frac{1}{2} \hat{T}^{\sim\varpi} (\widehat{\omega\alpha})^{\sim\varpi}}_{S_A^{\varpi}} + F_A^{\varpi}, \quad (1)$$

$$\frac{\partial K^{\varpi}}{\partial t} = \underbrace{-\nabla \cdot (\widehat{\mathbf{v}v_h}^{\sim\varpi} \widehat{\Phi}^{\sim\varpi})}_{\Delta Q_P^{\varpi}} + \underbrace{2 \left\{ (\widehat{\mathbf{v}v_h})^{\sim\varpi} : \nabla \widehat{\mathbf{v}v_h}^{\sim\varpi} - [\nabla \cdot (\widehat{\mathbf{v}v_h})^{\sim\varpi}] \cdot \widehat{\mathbf{v}v_h}^{\sim\varpi} \right\}}_{\Gamma_K^{\varpi}} + \underbrace{\left(-\nabla \cdot \left[\frac{1}{2} (\widehat{\mathbf{v}v_h})^{\sim\varpi} \cdot \widehat{\mathbf{v}v_h}^{\sim\varpi} \right] \right)}_{\Delta Q_K^{\varpi}} \\ + \underbrace{(-\hat{\omega}^{\sim\varpi} \hat{\alpha}^{\sim\varpi})}_{b^{\varpi}} + F_K^{\varpi}, \quad (2)$$

where $\mathbf{v} = (u, v, \omega)$ and the colon operator ($:$) in 2 is defined such that, for two dyadic products \mathbf{AB} and \mathbf{CD} , $(\mathbf{AB}) : (\mathbf{CD}) = (\mathbf{A} \cdot \mathbf{C})(\mathbf{B} \cdot \mathbf{D})$. The other notations are conventional. Note here Φ and α are anomalies. Their time averages have been removed a priori.

In the notations, the Q terms ΔQ_A^ϖ (ΔQ_K^ϖ) and ΔQ_P^ϖ are the convergence of the APE (KE) flux and pressure work, respectively—they represent the transport processes within the same window ϖ , the Γ -terms Γ_A^ϖ and Γ_K^ϖ are the transfers of APE and KE to window ϖ from other windows, b^ϖ is the rate of buoyancy conversion from APE to KE within window ϖ (positive if converted from APE to KE), S_A^ϖ is the apparent source/sink due to the vertical variation of statistic stability (usually negligible), and the F term F_A^ϖ (F_K^ϖ) represents the diffusion (dissipation) processes.

Note the expressions of the transfer and transport terms are completely different in form from their corresponding traditional counterparts. For the transfers Γ^ϖ (Γ_A^ϖ and Γ_K^ϖ), as proved by Liang (2016), they have a Lie bracket form and satisfy the Jacobian identity, reminiscent of the Poisson bracket in Hamiltonian dynamics. Moreover,

$$\sum_{\varpi} \sum_n \Gamma^\varpi = 0 \quad (3)$$

(note the suppressed subscript n in Γ^ϖ). This conservation property, though natural in appearance, does not hold with those transfers in traditional formalisms (see below). To distinguish, we call the Γ -like terms *canonical transfers*.

To see how a canonical transfer differs from its classical counterpart, consider a passive tracer T in an incompressible flow and neglect all other processes but advection:

$$\frac{\partial T}{\partial t} + \nabla \cdot (\mathbf{v}T) = 0. \quad (4)$$

Perform Reynolds decomposition: $T = \bar{T} + T'$ to arrive at the mean and perturbation energy equations (e.g., Pope, 2004)

$$\frac{\partial \bar{T}^2/2}{\partial t} + \nabla \cdot (\bar{\mathbf{v}}\bar{T}^2/2) = -\bar{T}\nabla \cdot (\bar{\mathbf{v}}'T'), \quad (5)$$

$$\frac{\partial \bar{T}'^2/2}{\partial t} + \nabla \cdot \left(\frac{\mathbf{v}\bar{T}^2}{2} \right) = -\bar{\mathbf{v}}'\bar{T}' \cdot \nabla \bar{T}. \quad (6)$$

The right-hand sides are generally understood as the respective energy transfers during the mean-eddy interaction. Particularly, when T is a velocity component, the right side of 6, $R = -\bar{\mathbf{v}}'\bar{T}' \cdot \nabla \bar{T}$, has been interpreted as the rate of energy extracted by Reynolds stress against the mean profile, which has been widely used in dynamic meteorology. Note that the right hands of 5 and 6 generally do not sum to zero. This is not what one would expect of an energy transfer, which by physical intuition should conserve energy as a whole; that is to say, they should sum to zero.

Based on the formalism in 1 and 2, the above does not make an issue. In this special case 5 and 6 are reduced to (see Liang, 2016)

$$\frac{\partial \bar{T}^2/2}{\partial t} + \nabla \cdot \left(\frac{1}{2}\bar{\mathbf{v}}\bar{T}^2 + \frac{1}{2}\bar{T}\mathbf{v}'T' \right) = -\Gamma, \quad (7)$$

$$\frac{\partial \bar{T}'^2/2}{\partial t} + \nabla \cdot \left(\frac{1}{2}\mathbf{v}\bar{T}^2 + \frac{1}{2}\bar{T}\mathbf{v}'T' \right) = \Gamma, \quad (8)$$

where

$$\Gamma = \frac{1}{2} \{ \bar{T}\nabla \cdot (\bar{\mathbf{v}}'T') - (\bar{\mathbf{v}}'T')\nabla \bar{T} \}. \quad (9)$$

Now the right-hand sides automatically sum to zeros, in sharp contrast to 5 and 6. To distinguish, we hence call this Γ a “canonical transfer.” As shown by Liang (2016), it has a Lie bracket form. Previously, Liang and

Robinson (2007) illustrated, for a benchmark barotropic instability model, the traditional Reynolds stress extraction $R = -\bar{\mathbf{v}}' \bar{T}' \cdot \nabla \bar{T}$ does not give the correct source of instability, while Γ does.

Note in a decomposition with more than two windows, a canonical transfer to a window ϖ may involve contributions from many windows. We need to differentiate the sources. Details are referred to Liang and Robinson (2005). Here we just use the superscript notation $\varpi_1 \rightarrow \varpi_2$ to signify the transfer from window ϖ_1 to ϖ_2 . It has been rigorously proved by Liang and Robinson (2007) that $\Gamma_A^{0 \rightarrow 1}$ provides a quantitative measure of the baroclinic instability of the mean flow, while $\Gamma_K^{0 \rightarrow 1}$ provides a barotropic instability measure. For convenience, in the following, we will write them as BC and BT and may refer to them as baroclinic transfer and barotropic transfer, respectively.

3. MWT Setup

The three scale windows for a process are demarcated in its wavelet spectrum by scale levels j_0, j_1 , and j_2 , with $2^{-j}, j = j_0, j_1, j_2$ being the corresponding normalized time scales. We first need to determine these scale levels or *window bounds*. The data we use for this study span 512 days from 22 March 2018 to 16 August 2019 with a time step of 6 hr, which total to 2^{11} steps. (MWT requires that the number of time steps be a power of 2.) This series has the cold wave period (January 2019) lying in the middle, with two ends far away enough to avoid the possible boundary effect. Through experiments, it is found that the CAO event can be clearly separated when the following parameters are selected:

$$j_0 = 3, \quad j_1 = 6, \quad j_2 = 11.$$

With these, the CAO is defined on a window with time scales from $2^{-6} \times 512 = 8$ to $2^{-(3+1)} \times 512 = 32$ days. We have also tried many other parameters, but this combination produces a CAO event in best agreement with that as reported; see Figures 1a–1c for a snapshot.

4. Results

4.1. The Cold Surge Actually Reflects a Stationary Wave Train

With the aforementioned setting, fields are reconstructed onto three scale windows, that is, the background window, the CAO window where lies the extreme cold wave event, and the synoptic window. Take the 500 hPa temperature as an example. The background temperature is shown in Figure 1b, which reveals a rather typical average pattern in boreal winter. The CAO-scale temperature is our focus. On 15 January, a cold air mass begins to move southward from the Arctic and reaches the Great Lakes on 21 January (see supporting information Movie S1b). It cuts off from the Arctic on 22 January and then stays over the region until 31 January (Figures 1c and 1d). The minimum of the CAO-scale temperature and the duration agree well with the center of the extreme event as reported by National Center for Atmospheric Research (cf. <https://www.climate.gov/news-features/blogs/beyond-data/bitterly-cold-extremes-warming-planet-putting-mid-west-late-january>). This validates our MWT parameter setting.

However, it is observed that, despite the cold center, there are actually two warm centers, one sitting over western North America and another over the Atlantic Ocean (e.g., Figures 1c and 1d). While this may not be clear on the original fields (Figure 1a), it indeed has been reported that “parts of western North America had warmer-than-average conditions” (<https://www.ncdc.noaa.gov/sotc/global/201901>). Moreover, these warm centers grow in time with the cold center and also keep their positions unchanged. So the January 2019 CAO over North America is actually a stationary wave localized over North America and Atlantic.

The above assertion is reconfirmed by the warming episode (3–10 February) immediately after the extremely cold days and another cooling then after (12–17 February; see Figures 1e and 1f). Correspondingly, the western and eastern flanks are cooled and warmed.

The evolution of the CAO-scale geopotential height resembles that of temperature (not shown) so does the CAO-scale velocity components (u^{-1}, v^{-1}), except that the center of v^{-1} has a westward shift and that of u^{-1} lies slightly northward (not shown). We have also examined the vertical profiles of these reconstructed fields over the Great Lakes region; the wave train extends upward over 300 hPa, with two deep warm highs and a

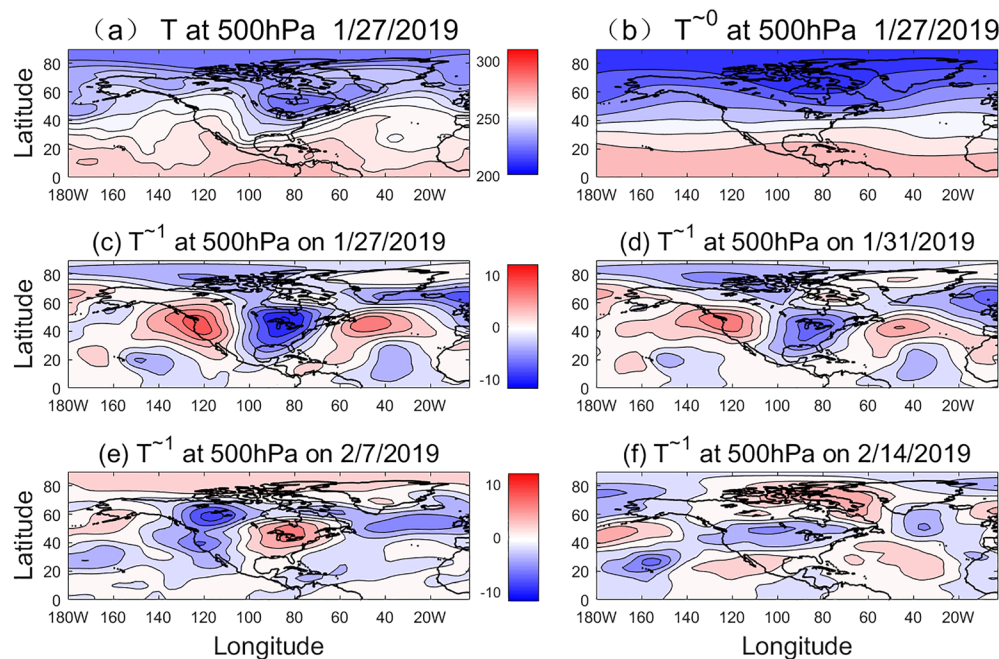


Figure 1. The 500 hPa temperature (K) (a) and its reconstructions on the background flow window (b) (contour interval: 4 K) and CAO-scale window (c) on 27 January 2019. (d), (e), and (f) are as (c) but on 31 January 2019, 7 February 2019, and 14 February 2019, respectively (contour interval: 2 K). A video is referred to Movie S1.

deep cold depression in between. Therefore, the January 2019 CAO is not just an isolated extremely cold event. Horizontally, the wave train structure must be taken into account. Temporally, the warming immediately following the cooling across much of the Midwest United States is an integrated part of this extreme event. That is to say, the alternative cooling-warming-cooling makes them a whole. With this observation, this event seems to be more attributed to the formation of a localized stationary wave train than the southward migration of an Arctic air mass. This will be clear soon below.

4.2. Formation of the Wave Train

So the January 2019 cold surge is actually a stationary wave localized over North America and Atlantic. Here naturally comes a question: How does this wave train form, and what are the dynamics underlying it? To study it, energy cycle diagnostics prove to be a powerful approach. Within a cycle, the interscale canonical transfers are of particular importance, as they provide quantitative measures of local hydrodynamic instabilities (Liang, 2016; Liang & Robinson, 2007). As we know from section 2, APE is approximately proportional to the square of the temperature on the same scale window. Therefore, the variation of the CAO-scale APE can be utilized to characterize the CAO. We hence pay special attention to the CAO-scale window energetics.

We integrate the energetics horizontally over the Arctic region from 60° to 85°N and over the wave train region from 22.5° to 60°N , 145° to 20°W and vertically from 850 to 200 hPa. (The pole is excluded as it is a singular point.) In doing this, we can trace where the CAO-scale APE is from. Notice that, as the integration is with respect to pressure, the resulting integrals should be divided by g , in order for it to have the units of energy change rate; same below (see Liang, 2016, for details).

By the sign of the time rate of the CAO-scale APE, that is, $\partial A^1 / \partial t$, the cold surge event is composed of an accelerated cooling episode (15–28 January, with a growing A^1) and a decelerated cooling episode (29–31 January, with a decaying A^1). During the former episode, buoyancy conversion and some other energetic processes also behave differently before and after 21 January. Accordingly, we can divide this extremely freezing event into three stages, namely, the wave train formation stage (15–21 January), the rapid growth stage (22–28 January), and the decay stage (29–31 January). In these stages the underlying dynamics are quite different. We choose some representative days to draw the energy flow charts. The results are shown in Figure 2.

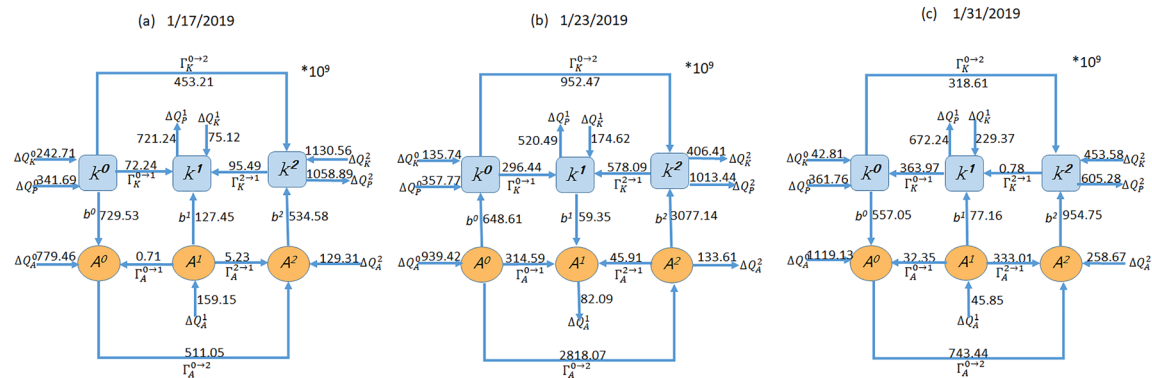


Figure 2. Typical multiscale energy cycles on typical days over the wave train region: (a) 17 January 2019, (b) 23 January 2019, and (c) 31 January 2019. Units: 10^9 W.

Figure 2a presents a typical chart of the energy flow for the initial formation stage (17 January). It is easy to see that, in this stage, the CAO-scale window gains APE (i.e., A^1) mainly via horizontal transport (ΔQ_A^1), in the amount of 159.15×10^9 W. This window loses APE to the background window by 0.71×10^9 W and to the synoptic window by 5.23×10^9 W. These plus the energy converted to K^1 on the same window (127.45×10^9 W) leave 25.76×10^9 W for A^1 to grow. Further analysis of ΔQ_A^1 indicates that it is mainly made of the southward flux from the Arctic. That is to say, it is the cold Arctic air masses that travel southward to North America and initialize the cooling. This is in agreement with the usual observation about the cold surge. We want to mention that not all the Arctic APE accounts for the cooling in this stage. A large part (127.45×10^9 W) is converted into the CAO-scale KE, causing the low-frequency fluctuation of the jet stream.

After 21 January, as shown in Figure 2b, the system enters a rapid growing stage, when the Arctic does not supply energy anymore— A^1 is now being transported out of the wave train region. But the CAO-scale window gains APE from both the background and synoptic windows and from the conversion of K^1 on the same window. On 23 January, these processes leave a balance of 337.76×10^9 W to feed A^1 . This causes the explosive growth of A^1 and hence the plummeting of temperature. Among these processes, overwhelmingly important is $\Gamma_A^{0 \rightarrow 1}$, that is, the baroclinic canonical transfer from the background window to the CAO-scale window, which makes 314.59×10^9 W (Figure 2b) of the total (337.76×10^9 W). By what we have presented in section 2, this means the explosive growth of the CAO-scale APE, that is, A^1 , hence the plummeting of temperature during this period, is due to a very strong baroclinic instability of the jet stream.

Of course, other processes also account for the growth of A^1 . The inverse cascade of APE from the synoptic storms and the buoyancy conversion from K^1 are two of them (Figure 2b). However, compared with the contribution from the baroclinic instability, their roles are secondary. Here we have two observations. First, during this period, $\Gamma_K^{0 \rightarrow 1}$, that is, the barotropic canonical transfer from the background window to the CAO-scale window, is also very large (296.44×10^9 W). So a strong barotropic instability is also happening then. However, the buoyancy conversion from K^1 to A^1 is rather limited (59.35×10^9 W), so its contribution to the temperature plummeting is not primary. The second observation is that the canonical transfers from the background window (Window 0) to the synoptic-scale window (Window 2) $\Gamma_A^{0 \rightarrow 2}$ and $\Gamma_K^{0 \rightarrow 2}$ are huge. Particularly, $\Gamma_A^{0 \rightarrow 2}$ is almost 1 order larger than what we are discussing about. But that does not account much for temperature variation, as A^2 is completely converted to K^2 , only leading to a very stormy weather. Besides, though a large part of K^2 is transferred upscale to the CAO-scale window (578.09×10^9 W), it does not contribute much to build up K^1 , as it is instantaneously transported away through pressure work (520.49×10^9 W). Putting all these together, clearly, it is the strong baroclinic instability that provides the primary APE for A^1 to grow. The strong barotropic instability and the weak upscale baroclinic canonical transfer, though significant, only play minor roles.

In the decay stage, as shown in Figure 2c, the A^1 -related energetics either become weak or change sign. Particularly, the mean flow now becomes baroclinically stable, with a weak negative canonical transfer (-32.35×10^9 W). A noteworthy process is the secondary baroclinic instability of the wave train, which

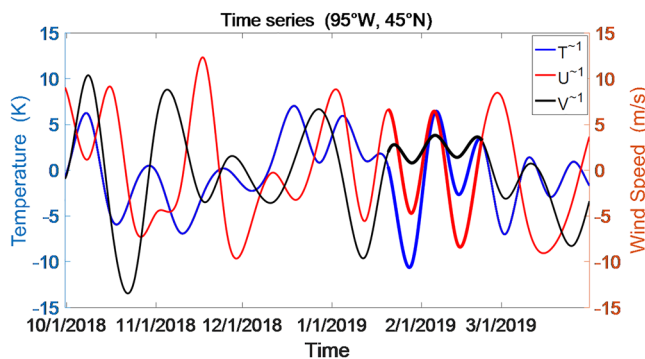


Figure 3. Evolutions of the CAO-scale temperature (red), zonal velocity (blue), and meridional velocity (black) at point (95°W, 45°N, 500 hPa). The thickened lines indicate the period when the three became synchronized. (Note the latter two already had been synchronized way before that.)

The synchronization between T , u , and v has important implications in fluid dynamics. As shown in section 2, the APE transferred from other scale windows to the CAO window is $\Gamma_A^1 = \frac{c}{2} [\widehat{(\mathbf{v}T)}^{\sim 1} \cdot \nabla \widehat{T}^{\sim 1} - \widehat{T}^{\sim 1} \nabla \cdot (\widehat{\mathbf{v}T})^{\sim 1}]$. By Liang and Anderson (2007), the product of two MWT transform coefficients $\hat{a}_n^{\sim 1} \hat{b}_n^{\sim 1}$ can be understood as the local correlation between a and b on the CAO-scale window. Besides, when only two scale windows are considered (i.e., ignore the synoptic-scale window) and when $j_0 = 0$, MWT is reduced to the classical Reynolds decomposition. For the purpose of illustration, we hence consider the problem within this simple framework. In this case, $T = \bar{T} + T'$, $\mathbf{v} = \bar{\mathbf{v}} + \mathbf{v}'$, and

$$\Gamma_A^1 = \frac{c}{2} [\overline{\mathbf{v}T' \nabla T'} - \overline{T' \nabla \cdot \mathbf{v}T'}],$$

which is $\Gamma_A^{0 \rightarrow 1}$ with a two-window decomposition and is reduced to (Liang & Robinson, 2007):

$$\frac{c}{2} [\overline{\mathbf{T} \nabla \cdot \mathbf{v}T'} - \overline{v' T' \cdot \nabla \bar{T}}] = \frac{c}{2} [\nabla \cdot (\overline{v' T' \bar{T}})] + c \left[-\overline{u' T'} \frac{\partial \bar{T}}{\partial x} - \overline{v' T'} \frac{\partial \bar{T}}{\partial y} \right].$$

Now we are considering the bulk energy transfer over the whole wave train region (vertically also integrated). The fluxes across the boundaries are negligible, so the first bracket vanishes by Gauss' theorem. In the second bracket, $\partial \bar{T} / \partial y$ is always negative, as the mean temperature poleward is lower. For $\partial \bar{T} / \partial x$, it is also negative. This is determined by the boreal winter circulation over North America, which is dominated by the U.S. East Coast trough, as reflected in Figure 1b. So, over North America, highly correlated CAO-scale velocity and temperature result in large $\overline{u' T'}$ and $\overline{v' T'}$ and hence large positive $\Gamma_A^{0 \rightarrow 1}$. That is to say, the synchronization between u' , v' , and T' maximizes $\Gamma_A^{0 \rightarrow 1}$, hence maximally extracting APE from the background to fuel the explosive CAO growth.

Note the measure of local baroclinic instability, namely, baroclinic canonical transfer $\Gamma_A^{0 \rightarrow 1}$, is always ahead of the CAO-scale APE, that is, A^1 (cf. Figure S1). This kind of lead-lag relation is actually ubiquitous in dynamical meteorology. In the supporting information, we present an illustration with the Eady edge wave model by Farrell (1985), which admits an analytical solution; see Figure S2. This is due to the fact that canonical transfer is the cause/drive and APE/KE is the effect/consequence and that *cause always precedes effect*. In the linear limit, this is expressed as lead-lag correlation, just as asserted in an explicit formula of a recent rigorous formalism of causality analysis (Liang, 2014). Now that the synchronization causes a maximized $\Gamma_A^{0 \rightarrow 1}$ and $\Gamma_A^{0 \rightarrow 1}$ causes an explosive growth of A^1 , which then leads to the severe cold surge, the synchronization hence can serve as a dynamic precursor for the extremely cold weather. Indeed, as shown in Figure 3, the synchronization leads the cold surge by more than 5 days.

transfers 333.01×10^9 W APE from the CAO window to the synoptic window. This is the major mechanism that leads to the decay of the cold surge.

4.3. A Remarkable Synchronization Between u , v , and T Maximizes the Baroclinic Instability

That a wave train is generated within the jet stream through baroclinic instability is not uncommon. But what makes the amplitude so large and hence an extremely freezing weather? To see this, we plot in Figure 3 the 500 hPa CAO-scale reconstructions of temperature, zonal velocity, and meridional velocity at point (95°W, 45°N), the center of the large stretch cooling. Remarkably, starting approximately on 20 January, the three fields begin to synchronize, and the synchronization lasts through 20 February; see the thickened segments of the three lines. (Notice that the synchronization between u and v actually begins early January, much earlier than that between u and T .)

5. Conclusions

To summarize, the January 2019 CAO over North America is not an isolated cold event. Horizontally, it is actually an extremely cold phase sandwiched within two abnormally warm phases. Temporally, the warming immediately following the cooling across much of the Midwest United States is also an integrated part of this extreme event. To gain insight into the dynamics, this stationary wave train structure (cf. Lindzen, 1986) must be taken into account.

A multiscale energetics study of the wave train reveals a three-stage process. In the first stage, it is formed with the needed APE supplied from the southward cold Arctic air. What causes the disaster to North America is in the second stage, that is, the rapid growth stage, during which the system is not related to Arctic anymore. Rather, it experiences a very strong baroclinic instability of the jet stream, which extracts energy from the background to fuel the explosive growth of the CAO-scale APE and hence the plummeting of the temperature. After a cooling-warming-cooling cycle, the surge eventually decays in the third stage, when we see a secondary baroclinic instability of the wave train which transfers APE from the cold surge window to the synoptic-scale window and then converts into the synoptic-scale KE, leading to a very stormy weather.

While it has been documented before that cold weather may be due to amplified planetary waves and that planetary waves can be amplified by baroclinic and/or barotropic instabilities, in this study we found that the very strong baroclinic instability is caused by a synchronization between u , v , and T on the CAO-scale window, a phenomenon identified in patches in many regions such as that around the Great Lakes. With a dynamical configuration like the winter circulation over North America (the U.S. East Coast trough, in particular), the remarkable synchronization maximizes the baroclinic canonical transfer and subsequently leads to the plummeting of temperature. As cause always precedes effect, the appearance of the synchronization heralds the arrival of the rapidly cooling episode.

One may ask why there appears such a synchronization. In complex systems, synchronization is a ubiquitous phenomenon which usually lasts forever once occurs, as evidenced in many networks made of dynamical oscillators. But here it can only be viewed as transient; so its appearance may be just occasional. In fact, such synchronization also appears in other regions, but no instability arises because there lacks the needed dynamical configuration such as the U.S. East Coast trough. We will examine this in detail in future studies.

Data Availability Statement

The data for this study are made available by NCEP/NCAR (<https://www.ersl.noaa.gov/psd/data/gridded/data.ncep.reanalysis.html>), and the information about the January 2019 cold surge is seen online (<https://www.climate.gov/news-features/blogs/beyond-data/bitterly-cold-extremes-warming-planet-putting-midwests-late-january>).

Acknowledgments

The constructive suggestions from Suzana Camargo and two anonymous reviewers are sincerely appreciated. F. X. thanks Yuanbing Zhao for his comments at the early stage of this work, and we thank the NUIST High Performance Computing Center for providing computational resources. This study is funded by National Science Foundation of China (41975064) and the 2015 Jiangsu Program for Innovation Research and Entrepreneurship Groups.

References

- Cai, M., Yu, Y. Y., Deng, Y., van den Dool, H. M., Ren, R. C., Saha, S., et al. (2016). Feeling the pulse of the stratosphere: An emerging opportunity for predicting continental-scale cold air outbreaks one month in advance. *Bulletin of the American Meteorological Society*, 97(8), 1475–1489. <https://doi.org/10.1175/BAMS-D-14-00287.1>
- Cattiaux, J., Vautard, R., Cassou, C., Yiou, P., Masson-Delmotte, V., & Codron, F. (2010). Winter 2010 in Europe: A cold extreme in a warming climate. *Geophysical Research Letters*, 37, L20704. <https://doi.org/10.1029/2010GL044613>
- Cellitti, M. P., Walsh, J. E., Rauber, R. M., & Portis, D. H. (2006). Extreme cold air outbreaks over the United States, the polar vortex, and the large-scale circulation. *Journal of Geophysical Research*, 111, D02114. <https://doi.org/10.1029/2005JD006273>
- Farrell, B. (1985). Transient growth of damped baroclinic waves. *Journal of the Atmospheric Sciences*, 42(24), 2718–2727. [https://doi.org/10.1175/1520-0469\(1985\)042%3C2718:TGODBW%3E2.0.CO;2](https://doi.org/10.1175/1520-0469(1985)042%3C2718:TGODBW%3E2.0.CO;2)
- Gao, Y., Leung, L. R., Lu, J., & Masato, G. (2015). Persistent cold air outbreaks over North America in a warming climate. *Environmental Research Letters*, 10, 044001. <https://doi.org/10.1088/1748-9326/10/4/044001>
- Harnik, N., Messori, G., Caballero, R., & Feldstein, S. B. (2016). The Circumglobal North American wave pattern and its relation to cold events in eastern North America. *Geophysical Research Letters*, 43, 11,015–11,023. <https://doi.org/10.1002/2016GL070760>
- Kodra, E., Steinhaeuser, K., & Ganguly, A. R. (2011). Persisting cold extremes under 21st-century warming scenarios. *Geophysical Research Letters*, 38, L08705. <https://doi.org/10.1029/2011GL047103>
- Konrad, C. E. (1996). Relationships between the intensity of cold-air outbreaks and the evolution of synoptic and planetary-scale features over North America. *Monthly Weather Review*, 124(6), 1067–1083. [https://doi.org/10.1175/1520-0493\(1996\)124%3C1067:rbitoc%3E2.0.co;2](https://doi.org/10.1175/1520-0493(1996)124%3C1067:rbitoc%3E2.0.co;2)
- Konrad, C. E. (1998). Persistent planetary scale circulation patterns and their relationship with cold air outbreak activity over the eastern United States. *International Journal of Climatology*, 18(11), 1209–1221. [https://doi.org/10.1002/\(SICI\)1097-0088\(199809\)18:11.3.CO;2-K](https://doi.org/10.1002/(SICI)1097-0088(199809)18:11.3.CO;2-K)

- Konrad, C. E., & Colucci, S. J. (1989). An examination of extreme cold air outbreaks over eastern North America. *Monthly Weather Review*, 117(12), 2687–2700. [https://doi.org/10.1175/1520-0493\(1989\)1172.0.CO;2](https://doi.org/10.1175/1520-0493(1989)1172.0.CO;2)
- Kretschmer, M., Coumou, D., Agel, L., Barlow, M., Tziperman, E., & Cohen, J. (2018). More-persistent weak stratospheric polar vortex states linked to cold extremes. *Bulletin of the American Meteorological Society*, 99(1), 49–60. <https://doi.org/10.1175/BAMS-D-16-0259.1>
- Lau, N. C., & Lau, K. M. (1984). The structure and energetics of midlatitude disturbances accompanying cold-air outbreaks over East Asia. *Monthly Weather Review*, 112(7), 1309–1327. [https://doi.org/10.1175/1520-0493\(1984\)112%3C1309:TSAEOM%3E2.0.CO;2](https://doi.org/10.1175/1520-0493(1984)112%3C1309:TSAEOM%3E2.0.CO;2)
- Liang, X. S. (2014). Unraveling the cause-effect relation between time series. *Physical Review E*, 90, 052150. <https://doi.org/10.1103/PhysRevE.90.052150>
- Liang, X. S. (2016). Canonical transfer and multiscale energetics for primitive and quasi-geostrophic atmospheres. *Journal of the Atmospheric Sciences*, 73(11), 4439–4468. <https://doi.org/10.1175/JAS-D-16-0131.1>
- Liang, X. S., & Anderson, D. G. M. (2007). Multiscale window transform. *SIAM Journal on Multiscale Modeling & Simulation*, 6(2), 437–467. <https://doi.org/10.1137/06066895X>
- Liang, X. S., & Robinson, A. R. (2005). Localized multiscale energy and vorticity analysis: I. Fundamentals. *Dynamics of Atmospheres and Oceans*, 38(3–4), 195–230. <https://doi.org/10.1016/j.dynatmoce.2004.12.004>
- Liang, X. S., & Robinson, A. R. (2007). Localized multiscale energy and vorticity analysis: II. Instability theory and validation. *Dynamics of Atmospheres and Oceans*, 44(2), 51–76. <https://doi.org/10.1016/j.dynatmoce.2007.04.001>
- Lindzen, R. S. (1986). Stationary planetary waves, blocking, and interannual variability. *Advances in Geophysics*, 29, 251–273. Elsevier. [https://doi.org/10.1016/S0065-2687\(08\)60042-4](https://doi.org/10.1016/S0065-2687(08)60042-4)
- Lorenz, E. N. (1955). Available potential energy and the maintenance of the general circulation. *Tellus*, 7, 157–167. <https://doi.org/10.1111/j.2153-3490.1955.tb01148.x>
- Pope, S. B. (2004). *Turbulent flows* (Vol. 12, No. 11, pp. 1–771). Cambridge University Press.
- Portis, D. H., Cellitti, M. P., Chapman, W. L., & Walsh, J. E. (2005). Low-frequency variability and evolution of North American cold air outbreaks. *Monthly Weather Review*, 134(2), 579–597. <https://doi.org/10.1175/mwr3083.1>
- Tomassini, L., Gerber, E. P., Baldwin, M. P., Felix, B., & Giorgetta, M. (2012). The role of stratosphere-troposphere coupling in the occurrence of extreme winter cold spells over northern Europe. *Journal of Advances in Modeling Earth Systems*, 4, m00A03. <https://doi.org/10.1029/2012MS000177>
- Van Oldenborgh, G. J., Haarsma, R., de Vries, H., & Allen, M. (2015). Cold extremes in North America vs. mild weather in Europe: The winter of 2013–14 in the context of a warming world. *Bulletin of the American Meteorological Society*, 96(5), 707–714. <https://doi.org/10.1175/BAMS-D-14-00036.1>
- Walsh, J. E., Phillips, A. S., Portis, D. H., & Chapman, W. L. (2001). Extreme cold outbreaks in the United States and Europe, 1948–99. *Journal of Climate*, 14(12), 2642–2658. [https://doi.org/10.1175/1520-0442\(2001\)014%3C2642:ECOITU%3E2.0.CO;2](https://doi.org/10.1175/1520-0442(2001)014%3C2642:ECOITU%3E2.0.CO;2)
- Xie, Z., Black, R. X., & Deng, Y. (2019). Planetary and synoptic-scale dynamic control of extreme cold wave patterns over the United States. *Climate Dynamics*, 53(3–4), 1477–1495. <https://doi.org/10.1007/s00382-019-04683-7>
- Yu, Y. Y., Ren, R. C., & Cai, M. (2015). Dynamic linkage between cold air outbreaks and intensity variations of the meridional mass circulation. *Journal of the Atmospheric Sciences*, 72(8), 3214–3232. <https://doi.org/10.1175/JAS-D-14-0390.1>